JOURNAL OF COMPUTATIONAL PHYSICS 25, 220–252 (1977)

Numerical Analysis of Blood Flow in the Heart

CHARLES S. PESKIN

Courant Institute of Mathematical Sciences, New York University, 251 Mercer Street, New York, New York 10012

Received October 14, 1976; revised February 14, 1977

The flow pattern of blood in the heart is intimately connected with the performance of the heart valves. This paper extends previous work on the solution of the Navier–Stokes equations in the presence of moving immersed boundaries which interact with the fluid. The boundary representation now includes the muscular heart wall. The fixed topology of the boundary representation is exploited in the solution of the nonlinear equations which implicitly define the boundary forces. An improved numerical representation of the δ-function is introduced. A fast Laplace-solver is used. The results of calculations with a natural valve and with a prosthetic valve are presented.

1. INTRODUCTION

The flow pattern of blood in the heart is intimately connected with the performance of the heart valves and is therefore of interest in the design of artificial valves and artificial hearts. In [1] we reported a numerical method for solving the Navier–Stokes equations in the presence of moving immersed boundaries (the heart-valve leaflets) which move at the local fluid velocity and exert forces locally on the fluid. This method has now been extended and improved in several ways.

We generalize the boundary representation so that it now includes not only the heart-valve leaflets but also the muscular heart wall. We use Newton's method to solve the equations which implicitly define the boundary forces, and we exploit the fixed topology of the boundary representation to generate an efficient Cholesky factorization of the relevant matrix. We introduce an improved numerical representation of the δ-function with remarkable properties which lead to approximate translation invariance in the interaction between boundary points. Finally, we retain Chorin's finite difference method for the Navier–Stokes equations [2], but we incorporate into this method the fast Laplace-solver of [3]. The possibility of using a fast Laplace-solver in a problem with moving boundaries of complicated geometry arises because of our representation of the boundary as a field of forces defined on the rectangular fluid mesh. The methods of this paper were reported in preliminary form in [4, 5] and a brief discussion of the corresponding experimental results is given in [6].

ISSN 0021-9991

2. Equations of Motion

The nonfluid parts of the heart, the valves and heart muscle, are incompressible and neutrally buoyant in blood. The mass density ρ is therefore a constant, and it is very attractive to use a single velocity field $\mathbf{u}(\mathbf{x}, t)$ with $\operatorname{div} \mathbf{u} = 0$ to describe the motion of the blood, valves, and heart muscle. The walls of the heart are moving, but it is convenient to have the velocity field $\mathbf{u}$ defined on a fixed domain. This can be accomplished by embedding the domain of interest in a larger periodic box and by regarding the part of this box exterior to the heart as being filled with fluid. The presence of this external fluid will have only a slight effect on the interior flow pattern, provided that the periodic box is big enough and that provision is made for external sources or sinks to accomodate the changes in volume which occur during the cardiac cycle because of inflow from the veins and outflow through the arteries. Because of the imposed periodicity in space, there are, in effect, no external boundaries, and we shall use the term "boundary" in the following to refer to the valves and heart muscle, which are internal boundaries.

Our aim is to write the equations of motion in a form which makes as little distinction as possible between the fluid and nonfluid regions. We must take account, however, of the extra forces acting in the valves and heart muscle. To describe these we introduce a force density $\mathbf{F}(\mathbf{x}, t)$ which differs from zero only on these nonfluid regions. (In case these nonfluid regions are represented as surfaces, $\mathbf{F}$ will be singular.) This notational device makes it possible to use the Navier–Stokes equations on the entire periodic domain Ω:

$$\rho(\partial_t \mathbf{u} + \mathbf{u} \cdot \nabla \mathbf{u}) = -\nabla p + \eta \Delta \mathbf{u} + \mathbf{F}, \tag{2.1}$$

$$\nabla \cdot \mathbf{u} = 0. \tag{2.2}$$

The calculation of the boundary force density $\mathbf{F}$ requires a knowledge of the configuration in space of the material points of the boundary. That is, we need a Lagrangian representation. The following notational device achieves this without the introduction of a coordinate system in the boundary. Moreover, it leads naturally to a numerical scheme.

Let a dense sequence of material sample points of the immersed boundary be labeled by the index $k = 1, 2, \ldots$, and let $\mathbf{x}_k$ be the position in space of the point k. Then $\{\mathbf{x}_k\}$ completely determines the configuration of the immersed boundary, the deformations of which are continuous.

Once a choice of the sample points $\{\mathbf{x}_k\}$ has been made, we can define the "boundary integral" of a function $\phi(\mathbf{x})$ over a region R:

$$\int_R \phi \, d\mu_B = \lim_{N \to \infty} \frac{1}{N} \sum_{k=1}^{N} \phi_k \delta_k(R), \tag{2.3}$$

where

$$\begin{aligned} \delta_k(R) &= 1, \ \mathbf{x}_k \in R \\ &= \int_R \delta(\mathbf{x} - \mathbf{x}_k) \, dv \\ &= 0, \ \mathbf{x}_k \notin R \end{aligned} \tag{2.4}$$

and where $\phi_k = \phi(\mathbf{x}_k)$. The value of this integral depends on the choice of sample points. The measure $\mu_B(R)$ defined by this choice is the fraction of sample points of the boundary which fall in the region R.

Now let $\mathbf{f}$ be the intensity of the boundary force with respect to this measure. That is, for an arbitrary region R, let

$$\begin{aligned}\int_R \mathbf{F}\, dv &= \int_R \mathbf{f}\, d\mu_B \\ &= \lim_{N\to\infty} \frac{1}{N} \sum_{k=1}^{N} \mathbf{f}_k \delta_k(R) \\ &\quad \lim_{N\to\infty} \frac{1}{N} \sum_{k=1}^{N} \mathbf{f}_k \int_R \delta(\mathbf{x} - \mathbf{x}_k)\, dv \\ &= \int_R \left[\lim_{N\to\infty} \frac{1}{N} \sum_{k=1}^{N} \mathbf{f}_k \delta(\mathbf{x} - \mathbf{x}_k)\right] dv.\end{aligned} \tag{2.5}$$

From this (formal) argument, since the region R is arbitrary, we conclude that

$$\mathbf{F}(\mathbf{x}) = \lim_{N\to\infty} \frac{1}{N} \sum_{k=1}^{N} \mathbf{f}_k \delta(\mathbf{x} - \mathbf{x}_k). \tag{2.6}$$

For fixed N, we represent the boundary force field as a sum of impulse functions applied at N distinct points. As $N \to \infty$, more and more impulses are used, and the intensity of each impulse diminishes accordingly. It is important to note that the limiting force field may or may not be singular depending on the number of dimensions of the "boundary" and of the space in which it is immersed. Let s be the number of space dimensions and b be the number of dimensions of the boundary. Then $\mathbf{F}(\mathbf{x})$ will be singular (in the limit $N \to \infty$) like a δ-function in $s - b$ dimensions, and nonsingular when $s = b$. We have assumed in the foregoing that the boundary has been sampled in such a way that $\mathbf{f}$ remains finite. That is, we have assumed that each portion of the boundary which is capable of exerting a finite force has been assigned nonzero measure by the sampling process.

For an elastic boundary, the boundary forces will depend on the boundary configuration. Thus

$$\mathbf{f}_k = \mathbf{f}_k(\mathbf{x}_1, \mathbf{x}_2, \ldots). \tag{2.7}$$

We also have the following equation of motion for the sample points of the boundary:

$$d\mathbf{x}_k/dt = \mathbf{u}(\mathbf{x}_k, t) = \int_{\mathbf{x}\in\Omega} \mathbf{u}(\mathbf{x}, t)\, \delta(\mathbf{x} - \mathbf{x}_k)\, dv, \tag{2.8}$$

the latter equality being simply the definition of the δ-function. Since the fluid is viscous, the velocity field is continuous across the immersed boundaries and (2.8) is not ambiguous.

We can summarize the equations of motion as follows:

$$\begin{aligned} \rho(\partial_t \mathbf{u} + \mathbf{u} \cdot \nabla \mathbf{u}) &= -\nabla p + \eta \Delta \mathbf{u} + \mathbf{F}, \\ \nabla \cdot \mathbf{u} &= 0, \\ d\mathbf{x}_k/dt = \mathbf{u}(\mathbf{x}_k, t) &= \int_{\mathbf{x} \in \Omega} \mathbf{u}(\mathbf{x}, t)\, \delta(\mathbf{x} - \mathbf{x}_k)\, dv, \\ \mathbf{F}(\mathbf{x}) &= \lim_{N \to \infty} (1/N) \sum_{k=1}^{N} \mathbf{f}_k \delta(\mathbf{x} - \mathbf{x}_k), \\ \mathbf{f}_k &= \mathbf{f}_k(\mathbf{x}_1, \mathbf{x}_2, \ldots). \end{aligned} \tag{2.9}$$

Note that the δ-function appears as a kernel in each of the equations in which a transition is made from boundary to fluid quantities or conversely. This expresses the local character of the interaction between the boundary and the fluid. Nevertheless, the boundary forces are felt instantaneously throughout the incompressible fluid. This comes about because $\nabla \cdot \mathbf{F}$ acts as a source for the pressure field.

3. Link Structures

The natural discretization of the boundary representation given above occurs simply by making N finite. In that case the configuration of the boundary is given by $\{\mathbf{x}_1 \cdots \mathbf{x}_N\}$ and the boundary forces are given by functions $f_k(\mathbf{x}_1 \cdots \mathbf{x}_N)$. We now restrict the form of these functions by assuming that the forces arise in straight-line segments connecting specified pairs of boundary points. Suppose that the link AB connects points A and B, and let

$$\mathbf{x}_{AB} = \mathbf{x}_B - \mathbf{x}_A, \tag{3.1}$$

$$L_{AB} = |\, \mathbf{x}_{AB} \,|, \tag{3.2}$$

$$T_{AB}(L_{AB}) = \text{tension in link } AB, \tag{3.3}$$

$$\mathbf{a}_{AB} = \mathbf{x}_{AB}/L_{AB}, \tag{3.4}$$

then,

$$(1/N)\, \mathbf{f}_A = \sum_{\substack{B=1 \\ B \neq A}}^{N} T_{AB} \mathbf{a}_{AB}. \tag{3.5}$$

We shall also need an expression for the changes in $\mathbf{f}_A$ that are produced (to first order) by a perturbation of the boundary configuration. This expression will have the form

$$d\mathbf{f}_A = N \sum_{\substack{B=1 \\ B \neq A}}^{N} Q_{AB}\, d\mathbf{x}_{AB}, \tag{3.6}$$

where Q_{AB} is an $s \times s$ matrix referring to the link AB, and $s = 2, 3$ is the number of space dimensions. The matrix Q_{AB} can be diagonalized by rotating to a system of coordinates in which the first coordinate is parallel to the link AB. In such a system, the first diagonal element is dT_{AB}/dL_{AB}, and the remaining diagonal elements are T_{AB}/L_{AB}. The following properties of the Q_{AB} matrices should be noted.

(i) If $T_{AB} \geqslant 0$ and $(dT_{AB}/dL_{AB}) \geqslant 0$, then $Q_{AB} \geqslant 0$. (Inequalities applied to a matrix will refer to the definiteness of the matrix. Thus $Q_{AB} \geqslant 0$ means Q_{AB} is positive semidefinite.)

(ii) For fixed AB, Q_{AB} is symmetric.

(iii) $Q_{AB} = Q_{BA}$

(iv) If $T_{AB} \equiv 0$ (that is, if there is no link between A and B), then $Q_{AB} = 0$.

Thus far, the Q_{AB} matrices are defined only for $A \neq B$. It will be useful, however, to introduce

$$Q_{AA} = -\sum_{\substack{B=1 \\ B \neq A}}^{N} Q_{AB}. \tag{3.7}$$

This allows us to rewrite (3.6) as

$$d\mathbf{f}_A = N \sum_{\substack{B=1 \\ B \neq A}}^{N} Q_{AB}(d\mathbf{x}_B - d\mathbf{x}_A) = N \sum_{B=1}^{N} Q_{AB}\, d\mathbf{x}_B. \tag{3.8}$$

The last summation has the form of matrix multiplication. Let f stand for the vector $(\mathbf{f}_1 \cdots \mathbf{f}_N)$ and let x stand for the vector $(\mathbf{x}_1 \cdots \mathbf{x}_N)$. Let Q be the $sN \times sN$ matrix constructed by writing the Q_{AB} blocks in their natural order. Then (3.8) may be written

$$(df) = NQ(dx). \tag{3.9}$$

If the off-diagonal blocks Q_{AB} are indeed $\geqslant 0$ (that is, if $dT_{AB}/dL_{AB} \geqslant 0$ and $T_{AB}/L_{AB} \geqslant 0$, all $A \neq B$), then the symmetric matrix $Q \leqslant 0$. This result has both physical and numerical significance which will be explained below. First, we give the proof. It is to be shown that $y^T Q y \leqslant 0$ for all y. Using (3.7) and the symmetry properties of Q, one can verify that

$$-y^T Q y = -\sum_{AB} \mathbf{y}_A \cdot Q_{AB}\mathbf{y}_B = +\frac{1}{2}\sum_{AB} (\mathbf{y}_A - \mathbf{y}_B) \cdot Q_{AB}(\mathbf{y}_A - \mathbf{y}_B). \tag{3.10}$$

But every term in the last summation is $\geqslant 0$, since the diagonal terms are zero and the off-diagonal blocks $Q_{AB} \geqslant 0$. Therefore, $y^T Q y \leqslant 0$ and $Q \leqslant 0$.

The physical significance of this result is that it implies $(df, dx) \leqslant 0$. This is a

stability condition, since it asserts that the forces generated by a perturbation oppose the perturbation. As an instructive example, consider a straight chain of links which satisfies $dT/dL > 0$. If the chain is under tension, $T > 0$, it is stable. Under compression, $T < 0$, the chain will buckle since perturbations away from the straight-line configuration produce forces which tend to increase the perturbation.

It is important to remark, however, that $T < 0$ does not always produce instability. For example, an equilateral triangle of links will be stable under tension or compression. The corresponding matrix Q will be negative semidefinite in both cases, even though the Q_{AB} blocks will be indefinite in the case of compression. This example shows that $Q_{AB} \geqslant 0$ for all $A \neq B$ is a sufficient, but not a necessary, condition for $Q \leqslant 0$.

We now discuss the numerical significance of the matrix Q constructed above. In order to secure numerical stability (see Section VII), we need to solve at each time step a system of equations of the form

$$\mathbf{x}_k^* = \mathbf{x}_k^0 + \lambda \mathbf{f}_k(\mathbf{x}_1^* \cdots \mathbf{x}_N^*), \tag{3.11}$$

where $\mathbf{x}_k^0$ and $\lambda > 0$ are given. The solution of this nonlinear fixed-point problem by Newton's method involves the factorization of the $sN \times sN$ matrix $I - \lambda NQ$. If the link structure is stable ($Q \leqslant 0$), then $I - \lambda NQ > 0$. We assume that this condition holds, and we use a Cholesky factorization of the matrix $I - \lambda NQ$.

The graph giving the block structure of $I - \lambda NQ$ is precisely the link structure of the boundary, with the boundary points as nodes and the links as edges. Although the boundary points move about in space, the topology is fixed. To preserve sparsity as much as possible during the factorization, we seek a numbering of the boundary points such that, in most cases, the points A and B are linked only if $|A - B|$ is small. The exceptional points are then numbered last. This results in a matrix with the structure shown in Fig. 1, a structure which is preserved during the factorization [7]. An example of a numbering with the desired properties is shown in Fig. 2.

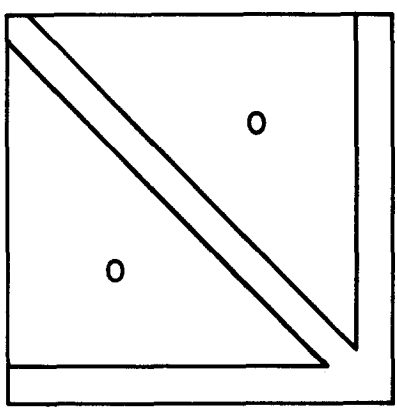

FIG. 1. The sparsity structure achieved by numbering the boundary points in such a manner that points k and l with $k < l \leqslant N$ are linked only if $(l - k)$ or $(N - l)$ is small.

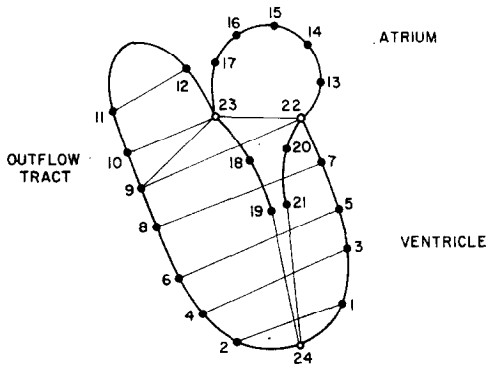

FIG. 2. An example of a numbering scheme with the required properties. The points 22–24, which are numbered last, constitute a separation set. Their deletion breaks up the boundary into four separate graphs, each of which has a matrix with a band structure. Note that the number of boundary points has been drastically reduced for clarity.

4. BOUNDARY FORCES

We shall now describe some specialized link structures which can be used in the representation of valve leaflets, heart muscle, and artificial valves. The properties of the material in question are, in effect, synthesized by the choice of an appropriate length–tension relation for each link and of an appropriate arrangement of the links in space.

Natural Heart Valve Leaflets

At present, in our two-dimensional calculations each valve leaflet appears as a chain of links, each link having a length–tension relation as follows:

$$\begin{aligned} T(L) &= (L - L_o)S, \qquad L > L_o\,, \\ &= 0, \qquad\qquad L \leqslant L_o\,, \end{aligned} \tag{4.1}$$

where S is the stiffness and L_o is the resting length. Alternatively, a nonlinear length–tension relation could be used without difficulty. In either case, the use of an instantaneous relation between length and tension reflects the fact that the valve leaflets are essentially elastic.

Heart Muscle

The phenomenological model of heart muscle used in this work is described in [8]. Models more closely related to the molecular mechanisms are also available [9], but the latter are far more complicated from the mathematical point of view. In the phenomenological model, each piece of heart muscle is represented as two springs

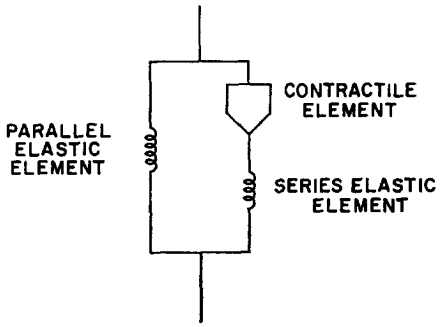

FIG. 3. The phenomenological model of heart muscle used in this work. The elastic elements satisfy instantaneous relations between length and tension, while the contractile element is characterized by a velocity of shortening which depends on the load [8].

and a "contractile element" arranged as in Fig. 3. The springs are characterized by functions T_P and T_A (which may be nonlinear) giving the instantaneous relation between length and tension. The contractile element is characterized by a velocity of shortening which depends on the active tension, on the length of the muscle, and on an activation parameter which we shall call α. Consequently, we have

$$T = T_P(L) + T_A(L - L_{CE}), \tag{4.2}$$

$$-dL_{CE}/dt = v(T_A, L, \alpha). \tag{4.3}$$

The activation parameter is a given function of time measured from the time of stimulation of the muscle. We therefore represent each segment of heart muscle by a pair of links of the type described above for the valve leaflets but with this important difference: In the active link, the resting length is reinterpreted as the contractile-element length, and it changes with time.

Note that the contractile-element length L_{CE} is not a given function of time. Instead it satisfies an ordinary differential equation in which L, the length of the link, appears. Thus L_{CE} depends indirectly on the motion of the fluid. An implicit scheme for this differential equation is

$$L_{CE}^{n+1} = L_{CE}^{n} - (\Delta t)v(T_A^{n+1}, L^{n+1}, \alpha^{n+1}), \tag{4.4}$$

where

$$T_A^{n+1} = T_A(L^{n+1} - L_{CE}^{n+1}). \tag{4.5}$$

Substituting (4.4) in (4.5) one eliminates L_{CE}^{n+1} and obtains a relation for length and tension for the active link at time $n + 1$. In this way we return to the general concept of a link with a given length–tension relation, but that relation is different at each time step. Moreover, the quantity L_{CE} for each active link must be stored and updated at each time step.

Artificial Valves

Typical prosthetic valves in current use have rigid, almost neutrally buoyant occluders, which move in a cage and alternately open and close the orifice guarded by the valve. Such an occluder can be represented as a link structure provided that

(i) the links resist compression as well as extension;

(ii) the arrangement of the links yields an overall structure which resists bending;

(iii) the stiffness is sufficiently large that the deformations are of no importance.

For example, a disk-type occluder in two-dimensional flow can be represented by the "railroad-bridge" structure of Fig. 4.

FIG. 4. A structure which resists bending, constructed from links which resist both compression and extension. We use this structure in the two-dimensional representation of a disk for an artificial valve.

5. DISCRETIZATION OF THE NAVIER–STOKES EQUATIONS

It will be shown below how the boundary forces are applied to the fluid mesh. Here we shall assume that this has already been done, and that the problem is to solve the Navier–Stokes equations with given force density $\mathbf{F}$ in a square, periodic box. For this purpose we use the method of Chorin [2], which will be briefly summarized here.

Introduce a square mesh of mesh width h and a time step k, and let $\mathbf{u}_{ij}^n$ and $\mathbf{F}_{ij}^n$ be the flow and force density evaluated at $t = nk$, $\mathbf{x} = (ih, jh)$. Let D_x^+, D_x^-, D_y^+, D_y^- be the forward and backward divided differences in the two space directions, e.g.,

$$(D_x^+\phi)_{ij} = h^{-1}(\phi_{i+1,j} - \phi_{ij}). \tag{5.1}$$

Also, let D_x^o, D_y^o be the centered divided differences, e.g.,

$$(D_x^o\phi)_{ij} = (2h)^{-1}(\phi_{i+1,j} - \phi_{i-1,j}). \tag{5.2}$$

Moreover, let

$$D\mathbf{u} = D_x^o u_x + D_y^o u_y = \nabla \cdot \mathbf{u} + O(h^2), \tag{5.3}$$

$$\mathbf{G}\phi = (D_x^o\phi, D_y^o\phi) = \nabla\phi + O(h^2). \tag{5.4}$$

With this notation, Chorin's scheme proceeds as follows:

$$\mathbf{u}^* = \mathbf{u}^n + k\mathbf{F}^n, \tag{5.5}$$

$$[I + k(u_x^n D_x^o - D_x^+ D_x^-)]\mathbf{u}^{**} = \mathbf{u}^*, \tag{5.6}$$

$$[I + k(u_y{}^n D_y{}^o - D_y{}^+ D_y{}^-)]\mathbf{u}^{***} = \mathbf{u}^{**}, \tag{5.7}$$

$$\mathbf{u}^{n+1} = \mathbf{u}^{***} - k\mathbf{G}p^{n+1}, \tag{5.8}$$

where p^{n+1} is chosen so that

$$D\mathbf{u}^{n+1} = 0. \tag{5.9}$$

Equations (5.6) and (5.7) are essentially one dimensional, since each contains differences in one space direction only. The corresponding matrix is tridiagonal except for an extra pair of elements introduced by the periodicity. The method used to solve such systems is discussed in [1].

The pair of equations (5.8)–(5.9) leads to the following equation for p^{n+1}:

$$k\, D\mathbf{G}\, p^{n+1} = D\mathbf{u}^{***}. \tag{5.10}$$

On a periodic domain with an even number of points in each space direction, Eq. (5.10) consists of four independent systems of equations, since only mesh points with the same parity in each coordinate are coupled. (For example, all mesh points having i even and j odd are coupled.) This is easily seen when we write out $D\mathbf{G}p$ as follows:

$$(D\mathbf{G}p)_{ij} = (4h^2)^{-1}(p_{i+2,j} + p_{i-2,j} + p_{i,j+2} + p_{i,j-2} - 4p_{ij}). \tag{5.11}$$

Each of the four systems is solved using the fast Laplace-solver of [3].

It is important to note that the boundary force field, which is not at all smooth, influences the entire flow instantaneously through its effect on the pressure field p. We can expect smooth results, then, only if each boundary point interacts equally with all four of the staggered meshes upon which p is calculated. These considerations will be very important in the next section.

6. Connecting the Boundary and Fluid Representations

The Lagrangian mesh upon which the boundary forces $\mathbf{f}_k$ and the boundary configuration $\mathbf{x}_k$ are stored has points which do not coincide with fluid mesh points. We therefore have the problem of interpolating the velocity field from the fluid mesh to the boundary points and spreading the boundary forces from the boundary points to the nearly mesh points of the fluid.

An indication of how this should be done comes from Eqs. (2.8) and (2.6) which have the natural discretization

$$\mathbf{u}_k = \sum_{ij} h^2 \mathbf{u}_{ij} D_{ij}(\mathbf{x}_k), \tag{6.1}$$

$$\mathbf{F}_{ij} = (1/N) \sum_k \mathbf{f}_k D_{ij}(\mathbf{x}_k), \tag{6.2}$$

where the kernel $D_{ij}(\mathbf{x}_k)$, which corresponds to $\delta(\mathbf{x} - \mathbf{x}_k)$, remains to be constructed.

Let $\mathbf{x} = (x, y)$ and let

$$D_{ij}(\mathbf{x}) = d(x - ih)\, d(y - jh), \tag{6.3}$$

where

$$\begin{aligned} d(r) &= (1/4h)(1 + \cos(\pi r/2h)), && |\, r\,| < 2h, \\ &= 0, && |\, r\,| \geqslant 2h. \end{aligned} \tag{6.4}$$

The shape of this function is shown in Fig. 5.

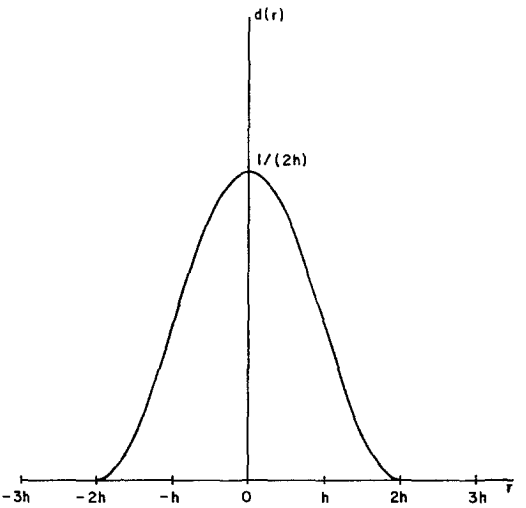

FIG. 5. Numerical representation of the δ-function.

The function $d(r)$ satisfies the following conditions:

$$\sum_i hd(x - ih) = \int_{-\infty}^{\infty} d(x)\, dx = 1, \tag{6.5}$$

$$d(x) = 0 \quad \text{when} \quad |\, x\,| \geqslant 2h, \tag{6.6}$$

$$d(x) = d(-x), \tag{6.7}$$

$$\sum_{i \text{ even}} hd(x - ih) = \sum_{i \text{ odd}} hd(x - ih) = \tfrac{1}{2}, \tag{6.8}$$

$$\sum_i hd(x_1 - ih)\, d(x_2 - ih) \leqslant \sum_i hd^2(x - ih) = 3/8h. \tag{6.9}$$

The properties (6.5)–(6.7) guarantee that d corresponds to the δ-function. For

example, if ϕ_i are the samples of a continuous function ϕ on a mesh of mesh width h, we have as a consequence of these properties

$$\lim_{h\to 0} \sum_i hd(x - ih)\phi_i = \phi(x). \tag{6.10}$$

The additional property (6.8) guarantees that any boundary point interacts equally with all four of the staggered meshes upon which the pressure field is calculated (see Eq. (5.11)).

The property (6.9) is the most interesting. To understand its importance consider the interaction between pairs of boundary points as transmitted through the fluid. Such an interaction will involve the double interpolation of a discrete, translation invariant, Green's function. For simplicity, we study such a double interpolation in one dimension. Let $g(i_1 - i_2)$ be the discrete Green's function giving the influence of mesh point i_1 on i_2. Then we construct $\tilde{g}(x_1, x_2)$ as follows:

$$\tilde{g}(x_1, x_2) = \sum_{i_1 i_2} h^2 d(x_1 - i_1 h)\, g(i_1 - i_2)\, d(x_2 - i_2 h) \tag{6.11}$$

$$= \sum_i hg(i) \sum_{i_1} hd(x_1 - i_1 h)\, d(x_2 + ih - i_1 h), \tag{6.12}$$

where $i = i_1 - i_2$.

According to the property (6.9), the coefficient of $g(i)$ now achieves a unique maximum value when $x_1 - x_2 = ih$, independent of the individual positions of the points x_1 and x_2.

Remark. This is not complete translation invariance. We would like to have $\tilde{g}$ itself depend only on $x_1 - x_2$. To achieve this for arbitrary $g(i_1 - i_2)$ it would be necessary to have some relation of the form

$$\sum_i hd(x_1 - ih)\, d(x_2 - ih) = f(x_1 - x_2). \tag{6.13}$$

Indeed such a relation holds for the δ-function itself, since we have

$$\int \delta(x_1 - x)\, \delta(x_2 - x)\, dx = \delta(x_1 - x_2). \tag{6.14}$$

Unfortunately, however, Eq. (6.13) is incompatible with the finite support of the function d. To see this, choose $| x_1 - x_2 |$ such that the support of $d(x_1 - ih)\, d(x_2 - ih)$ has length $h/2$. Then the sum in Eq. (6.13) has at most one nonzero term. Now if we translate x_1 and x_2, holding $x_1 - x_2$ constant, we can always find places where there is one nonzero term and others where there are none. Consequently, the sum in Eq. (6.13) cannot depend only on $x_1 - x_2$ when the function d has finite support.

We have listed above certain properties of the function $d(r)$. One may also ask to what extent these properties uniquely determine the function. In this connection we first note that some of the properties are consequences of the others. In particular,

Eq. (6.5) is a consequence of (6.8) and the inequality in (6.9) is a consequence of the equality in (6.9) because of the Schwarz inequality. The fact that the constant in (6.9) is $3/8h$ is also a consequence of the other properties. As a minimal set of properties we may therefore take (6.6)–(6.8) and

$$\sum_i hd^2(x - ih) = \text{constant, independent of } x. \tag{6.15}$$

One can then verify that these conditions alone determine the function $d(r)$ uniquely at the points $| r | = 0, h/2, h, 3h/4, 2h$ and, of course on $| r | \geqslant 2h$. Moreover, if the function $d(r)$ is given on $0 \leqslant r \leqslant h/2$, then its continuation to the rest of the real line is uniquely determined. Thus the stated conditions severely restrict the choice of the function $d(r)$, and (6.4) seems like the simplest choice compatible with these conditions.

7. Numerical Stability

In Section 5, Chorin's scheme for the Navier–Stokes equations was summarized with $\mathbf{F}$ given. In the present problem, $\mathbf{F}$ is very sensitive to boundary configuration, and an implicit scheme is needed to secure numerical stability. Fortunately, it is enough to use an implicit fractional step. That is, we compute the boundary forces not from the final configuration $\mathbf{x}^{n+1}$ but from a configuration $\mathbf{x}^*$ defined implicitly as follows:

$$\mathbf{x}_k{}^* = \mathbf{x}_k{}^n + \Delta t \mathbf{u}_k{}^*, \tag{7.1}$$

$$\mathbf{u}_{ij}^* = \mathbf{u}_{ij}^n + \Delta t \mathbf{F}_{ij}^*, \tag{7.2}$$

where

$$\mathbf{u}_k{}^* = \sum_{ij} h^2 D_{ij}(\mathbf{x}_k{}^n)\mathbf{u}_{ij}^*, \tag{7.3}$$

$$\mathbf{F}_{ij}^* = (1/N) \sum_k \mathbf{f}_k(\mathbf{x}_1{}^* \cdots \mathbf{x}_N{}^*)\, D_{ij}(\mathbf{x}_k{}^n). \tag{7.4}$$

Substituting, we find the following equation for $\mathbf{x}^*$:

$$\mathbf{x}_k{}^* = \mathbf{x}_k{}^n + \Delta t \mathbf{u}_k{}^n + ((\Delta t)^2/N) \sum_l \sum_{ij} h^2 D_{ij}(\mathbf{x}_l{}^n)\, D_{ij}(\mathbf{x}_k{}^n)\, \mathbf{f}_l(\mathbf{x}_1{}^* \cdots \mathbf{x}_N{}^*). \tag{7.5}$$

The quantity

$$\begin{aligned} \sum_{ij} h^2 D_{ij}(\mathbf{x}_l{}^n)\, D_{ij}(\mathbf{x}_k{}^n) &= 9/64h^2, && k = l, \\ &= < 9/64h^2, && k \neq l, \\ &= 0, && | x_k{}^n - x_l{}^n | \geqslant 4h \text{ or } | y_k{}^n - y_l{}^n | \geqslant 4h. \end{aligned} \tag{7.6}$$

It is therefore a reasonable approximation to replace this quantity by $\beta(9/64h^2)\delta_{kl}$, where β is an adjustable parameter of order 1. In that case Eq. (7.5) takes the following form in which all reference to the fluid mesh has disappeared:

$$\mathbf{x}_k^* = \mathbf{x}_k^o + \lambda \mathbf{f}_k(\mathbf{x}_1^* \cdots \mathbf{x}_N^*), \tag{7.7}$$

where

$$\mathbf{x}_k^o = \mathbf{x}_k^n + \Delta t \mathbf{u}_k^n = \text{known quantity at beginning of } n\text{th time step}, \tag{7.8}$$

$$\lambda = \frac{9}{64h^2} \frac{(\Delta t)^2}{N} \beta. \tag{7.9}$$

We remark that if $\Delta t = O(h^2)$ and $N = O(h^{-1})$, then $\lambda = O(h^3)$. Consequently, as $h \to 0$, $\mathbf{x}_k^* \to \mathbf{x}_k^o \to \mathbf{x}_k^n$ and $\mathbf{f}_k \to \mathbf{f}_k(\mathbf{x}_1^n \cdots \mathbf{x}_N^n)$.

The method for solving Eq. (7.7) was discussed in Section 3. Once this problem is solved the forces are regarded as known and no further use is made of the boundary configuration $\{\mathbf{x}_k^*\}$.

8. Sources and Sinks

Our specific application in this work is the flow of blood on the left side of the heart during ventricular diastole and early systole. This flow is influenced by the return of blood to the left atrium through the pulmonary veins. To model this venous return we put a source in the middle of the atrium and a corresponding sink exterior to the heart to absorb the volume displaced by the moving walls. In this section we first specify the nature of the source, and then show how its presence alters the numerical method.

It will be very convenient to have the source strength determined at any instant by a single quantity Q, the volume rate of flow. Thus, we write instead of $\nabla \cdot \mathbf{u} = 0$,

$$\nabla \cdot \mathbf{u} = \psi(\mathbf{x}, t) = Q(t)\, \psi_o(\mathbf{x}) \tag{8.1}$$

Since the domain is periodic, the integral of $\nabla \cdot \mathbf{u}$ is identically zero, and

$$\int_{\mathbf{x} \in \Omega} \psi_o(\mathbf{x})\, dv = 0. \tag{8.2}$$

Equation (8.2) is the mathematical reason why a sink is needed corresponding to the atrial source. To specify the spatial distribution of the source and the sink, introduce two nonnegative functions w_a and w_e with integral 1, and let

$$\psi_o(\mathbf{x}) = w_a(\mathbf{x} - \mathbf{X}_a) - w_e(\mathbf{x}), \tag{3.8}$$

where $\mathbf{X}_a$ is a point in the middle of the left atrium. The support of $w_e(\mathbf{x})$ is exterior

to the heart (actually, near the edges of the domain), and the support of $w_a(\mathbf{x} - \mathbf{X}_a)$ is in the atrium.

Since w_a and w_e are weight functions, it is natural to define the average pressures at the source and the sink as

$$P_a(t) = \int_{\mathbf{x}\in\Omega} p(\mathbf{x}, t)\, w_a(\mathbf{x} - \mathbf{X}_a)\, dv, \tag{8.4}$$

$$P_e(t) = \int_{\mathbf{x}\in\Omega} p(\mathbf{x}, t)\, w_e(\mathbf{x})\, dv. \tag{8.5}$$

Thinking of $P_e(t)$ as a reference pressure, we define

$$P_{\text{atrium}} = P_a - P_e = \int_{\mathbf{x}\in\Omega} p(\mathbf{x}, t)\, \psi_o(\mathbf{x})\, dv = (\psi_o\,, p), \tag{8.6}$$

and we note that P_{atrium} is unchanged if a constant is added to the pressure field.

We specify $Q(t)$ in terms of $P_{\text{atrium}}(t)$ in the following way

$$Q(t) = Q_s - \alpha_s P_{\text{atrium}}(t), \tag{8.7}$$

where Q_s and α_s are constants. This amounts to a linear resistance model of the flow of blood through the pulmonary veins.

Substituting (8.7) and (8.6) in (8.1), we find

$$\nabla \cdot \mathbf{u} = \psi_o(\mathbf{x})\,\{Q_s - \alpha_s(\psi_o\,, p)\}. \tag{8.8}$$

To accommodate this source, the numerical solution of the Navier–Stokes equations (Section 5) is modified as follows. Instead of Eqs. (5.9) and (5.10), we have

$$D\mathbf{u}^{n+1} = \psi_o\{Q_s - \alpha_s(\psi_o\,, p^{n+1})_h\}, \tag{8.9}$$

$$kD\mathbf{G}p^{n+1} = D\mathbf{u}^{***} - \psi_o\{Q_s - \alpha_s(\psi_o\,, p^{n+1})_h\}, \tag{8.10}$$

where

$$(f, g)_h = \sum_{ij} h^2 f_{ij}\, g_{ij}\,. \tag{8.11}$$

Equation (8.10) is easily solved at the expense of two calls to a fast Laplace-solver. First solve for p_0 and p_1 which are defined (up to a constant) by

$$kD\mathbf{G}p_0 = \psi_o Q_s\,, \tag{8.12}$$

$$kD\mathbf{G}p_1 = D\mathbf{u}^{***}. \tag{8.13}$$

By linearity, p^{n+1} will have the form

$$p^{n+1} = p_1 - \lambda p_o\,, \tag{8.14}$$

where

$$\lambda Q_s = \{Q_s - \alpha_s(\psi_o\,, p^{n+1})_h\}. \tag{8.15}$$

Substituting (8.14) in (8.15) and solving for λ we get

$$\lambda = \frac{Q_s - \alpha_s(\psi_o\,,\, p_1)_h}{Q_s - \alpha_s(\psi_o\,,\, p_o)_h}\,. \tag{8.16}$$

Since $D\mathbf{G}$, the discrete Laplacian, is a nonpositive operator, we see from (8.12) that $(\psi_o\,,\, p_o)_h \leqslant 0$. The denominator in the expression for λ is therefore bounded away from zero. Also, since $(\psi_o\,,\, 1)_h = 0$, λ is uniquely determined despite the fact that p_o and p_1 are only defined up to a constant.

All of the expressions in this section remain valid if ψ_o depends on t as well as $\mathbf{x}$. This will actually be the case since the atrium moves during the cardiac cycle. Equation (8.12) must therefore be solved anew at each time step, and the presence of the source doubles the amount of time spent solving Laplace's equation. It should be mentioned, however, that for a fixed source Eq. (8.12) could be solved once, and p_o could be stored on the disk. In that case, the extra computational effort associated with the source would be very small.

9. Summary of the Numerical Scheme

At each time step, a boundary configuration $\mathbf{x}_k{}^n$ and a fluid velocity field $\mathbf{u}_{ij}$ are given. The construction of $\mathbf{x}^{n+1}$ and $\mathbf{u}^{n+1}$ proceeds as follows:

$$\mathbf{x}_k{}^* = [\mathbf{x}_k{}^n + (\Delta t)\mathbf{u}_k{}^n] + \lambda \mathbf{f}_k(\mathbf{x}_1{}^* \cdots \mathbf{x}_N{}^*), \tag{9.1}$$

$$F_{ij}^* = (1/N) \sum_k \mathbf{f}_k(\mathbf{x}_1{}^* \cdots \mathbf{x}_N{}^*)\, D_{ij}(\mathbf{x}_k{}^n), \tag{9.2}$$

$$\mathbf{u}^* = \mathbf{u}^n + (\Delta t)\mathbf{F}^*, \tag{9.3}$$

$$\{I + (\Delta t)(u_x{}^n D_x{}^o - D_x{}^+ D_x{}^-)\}\mathbf{u}^{**} = \mathbf{u}^*, \tag{9.4}$$

$$\{I + (\Delta t)(u_y{}^n D_y{}^o - D_y{}^+ D_y{}^-)\}\mathbf{u}^{***} = \mathbf{u}^{**}, \tag{9.5}$$

$$(\Delta t)\, D\mathbf{G}p^{n+1} = D\mathbf{u}^{***} - \psi_o\{Q_s - \alpha_s(\psi_o\,,\, p^{n+1})_h\}, \tag{9.6}$$

$$\mathbf{u}^{n+1} = \mathbf{u}^{***} - (\Delta t)\,\mathbf{G}p^{n+1}, \tag{9.7}$$

$$\mathbf{x}_k^{n+1} = \mathbf{x}_k{}^n + (\Delta t) \sum_{ij} h^2 D_{ij}(\mathbf{x}_k{}^n)\mathbf{u}_{ij}^{n+1}. \tag{9.8}$$

In the foregoing, step (9.1) involves the solution of a nonlinear system of equations, and steps (9.4) through (9.6) involve the solution of linear systems. The methods of solution have been discussed above.

10. Results: Flow Patterns of the Mitral Valve

The mitral valve is the inflow valve to the left ventricle. Blood returning from the lungs to the heart enters the left atrium, from which it is transferred to the left ventricle across the mitral valve. In order to study the flow patterns of the mitral valve, we

need to construct a representation of the heart which includes at least the left atrium and the left ventricle. These will be constructed out of muscular and elastic links, as described above, arranged in the two-dimensional geometry shown in Fig. 2. This arrangement resembles a cross section of the left heart in a plane which bisects the two major leaflets of the mitral valve and which also passes through the apex of the heart. The orientation of this plane is indicated in Fig. 6.

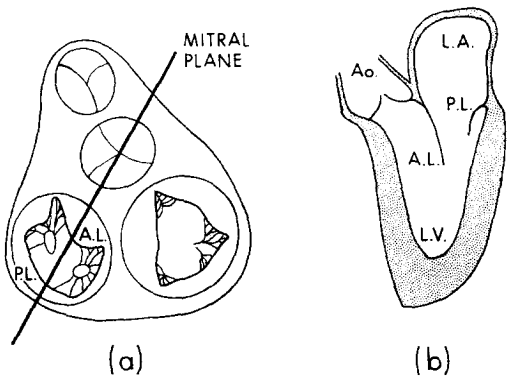

FIG. 6. (a) Base of the heart, showing the orientation of the mitral plane, which bisects the two major leaflets of the mitral valve and which contains the apex of the left ventricle. (b) Left heart structures of the mitral plane: L.A. = left atrium, L.V. = left ventricle, Ao. = aorta, A.L., P.L. = anterior and posterior leaflets of the mitral valve.

There are several aspects of cardiac anatomy which do not appear directly in this plane but which nevertheless cannot be neglected. These are represented by crosslinks in the model. (By a crosslink we mean a link whose length is independent of the mesh width.) For example, the papillary muscles and chordae tendinae which support the mitral valve lie on either side of the plane of interest. Each muscle has chordae which attach to both leaflets near the commissures. We represent this on the model by crosslinks from the tips of the leaflets to the point which represents the apex of the heart.

Similarly, the circular muscle in the wall of the ventricle near the equatorial plane cannot appear directly in the model, but the resultant force it exerts on the fluid is inward. This muscle can therefore be represented by crosslinks from one side of the ventricle to the other. The shapes of the outflow tract and of the atrioventricular ring are also maintained by cross-links.

In the case of the atrioventricular ring we use crosslinks which represent a mixture of atrial and ventricular muscle. This corresponds to the physiological observation that the ring begins to contract during atrial systole and continues to contract during ventricular systole. Incidently, when passive elastic crosslinks were tried for the atrioventricular ring, we found a remarkable expansion of the ring during ventricular systole which interfered with effective closure of the mitral valve.

Inflow to the left atrium from the pulmonary veins is supplied in the model by a source in the middle of the atrial chamber. We assume that the inflow has the form

$(Q_s - \alpha_s P_{\text{atrium}})$, where Q_s and α_s are constants. A corresponding sink near the edges of the mesh (outside the heart) absorbs the external fluid displaced by changes in cardiac volume. At the present time, we have not included an aortic valve in the model, and we restrict our calculations to that part of the cardiac cycle when the aortic valve is closed. We have, however, included an outflow tract in the ventricular geometry, since this feature of ventricular anatomy is important to the function of the anterior leaflet of the mitral valve. (In particular, it allows room for a strong vortex to form behind the anterior leaflet. This vortex participates in valve closure [10, 11].)

The timing and the strength of contraction of the atrial and ventricular muscle are controlled in the model by specifying the state of activation for each type of muscle as a given function of time. At the present time, we supply one such activation function for the atrial muscle and another for the ventricular. This allows for a delay between the contraction of the atrium and the ventricle, but it means that all parts of the atrium contract simultaneously and then that all parts of the ventricle contract simultaneously. In fact, the most important delay in the conduction of the cardiac impulse occurs at the junction of the atrium and the ventricle, but it would also be possible to include in the model the smaller delays which occur during the spread of excitation over the atrium or over the ventricle.

The physical quantities which set the scale for the fluid dynamics of the human mitral valve are as follows:

$$\begin{aligned} L_o &= \text{diameter of the mitral ring} = 3.2 \text{ cm}; \\ T_o &= \text{duration of a heartbeat} = 0.86 \text{ sec}; \\ \nu &= \text{kinematic viscosity of blood} = 0.04 \text{ cm}^2/\text{sec}. \end{aligned}$$

These can be combined into a dimensionless parameter

$$R_o = L_o^2/\nu T_o \cong 3 \times 10^2. \tag{10.1}$$

This parameter is closely related to the usual Reynolds number LU/ν, where U is a typical velocity of the flow. To make the connection simply note that the fluid motion is generated by the walls of the heart. The motions of the walls occur through distances of order L in times of order T. Thus U has the same order of magnitude as L/T.

In the present work we reduce the Reynolds number by setting $L = \gamma L_o$, $T = \gamma T_o$ so that $R = \gamma R_o$. The results presented here were computed with $\gamma = 0.01$. The factor γ is introduced to make the problem computationally tractable, since the finite difference method requires a mesh width which is inversely proportional to the Reynolds number [2]. We like to think that the introduction of this factor is justified by the comparative physiology of the hearts of different mammals. There is some evidence, reviewed by this author in [5], that the hearts of different mammals are roughly scale models of each other and that L is roughly proportional to T. The largest mammals have Reynolds numbers about 100 times greater than the smallest mammals. This suggests the hypothesis that the essential features of cardiac fluid dynamics are not very sensitive to Reynolds number. Of course, this point should be

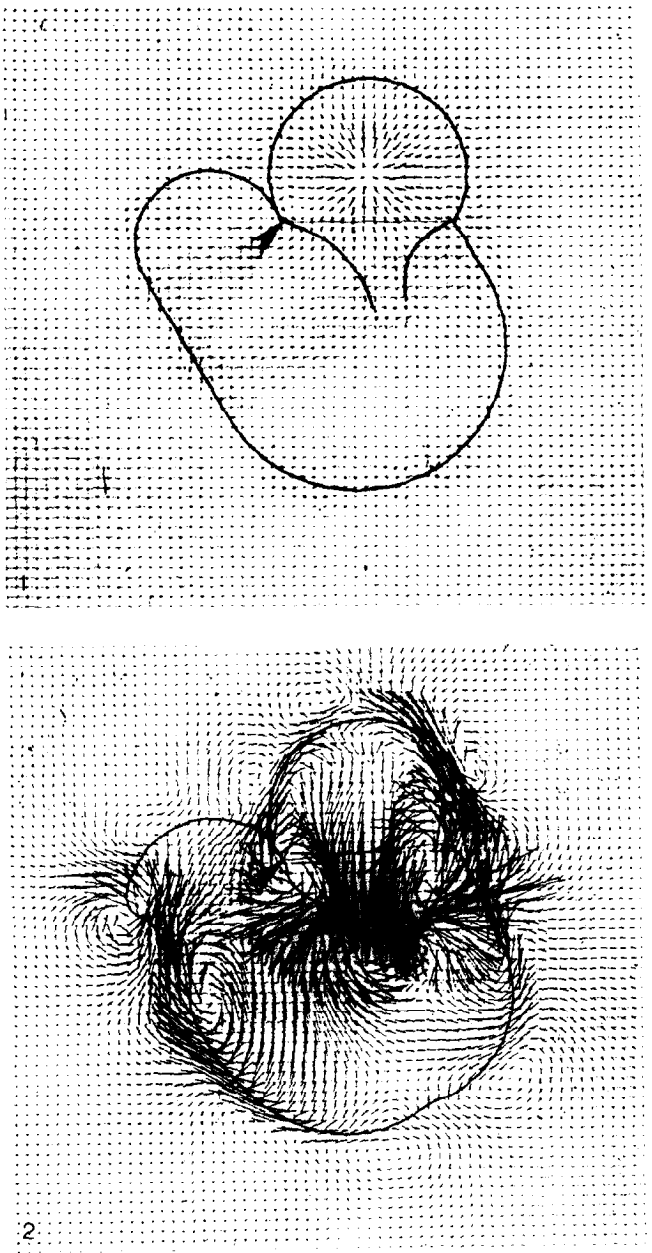

FIG. 7. Flow patterns of the mitral valve. Frames 1–7, relaxation of the ventricle. Frames 8–11, contraction of the atrium. Frame 12, contraction of the ventricle. Note the pattern of valve opening, vortex formation, and partial valve closure by the vortex streamlines which occurs during relaxation of the ventricle and which is repeated during the contraction of the atrium. Vortex formation occurs at the cusp margins. Backflow in frame 12 consists of fluid displaced by the moving cusps, as the flow is still in the forward direction at and below the cusp margins.

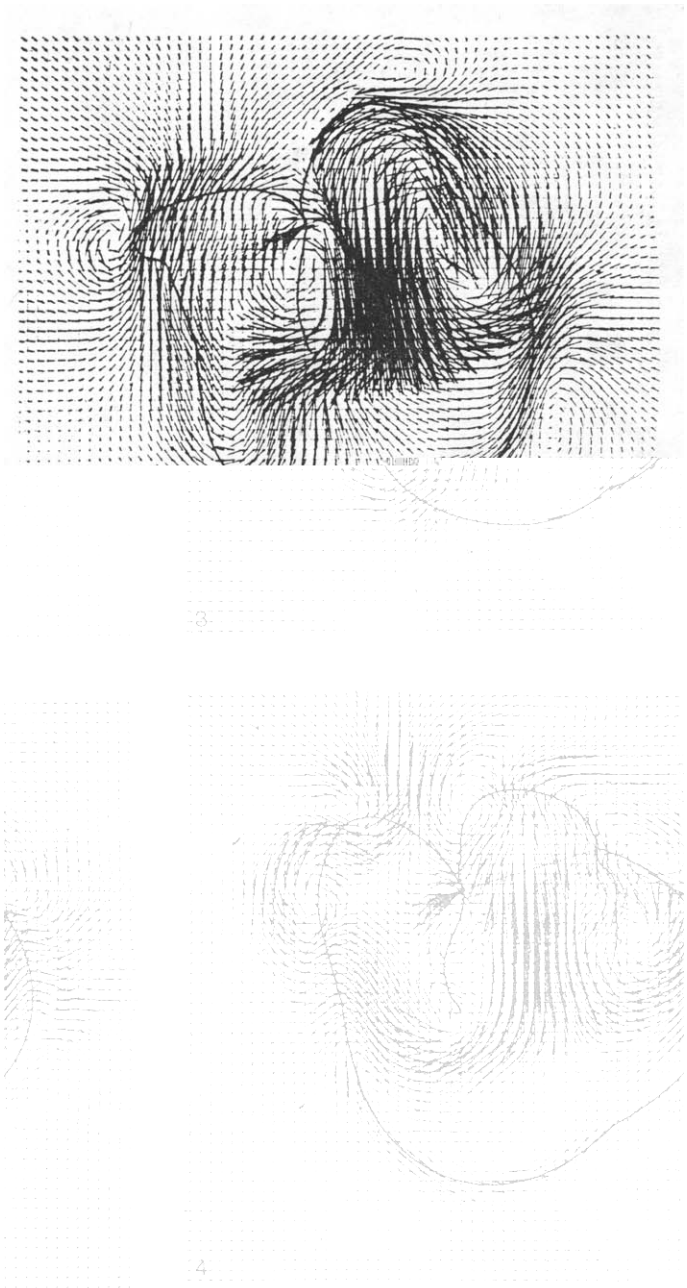

FIG. 7. *Continued.*

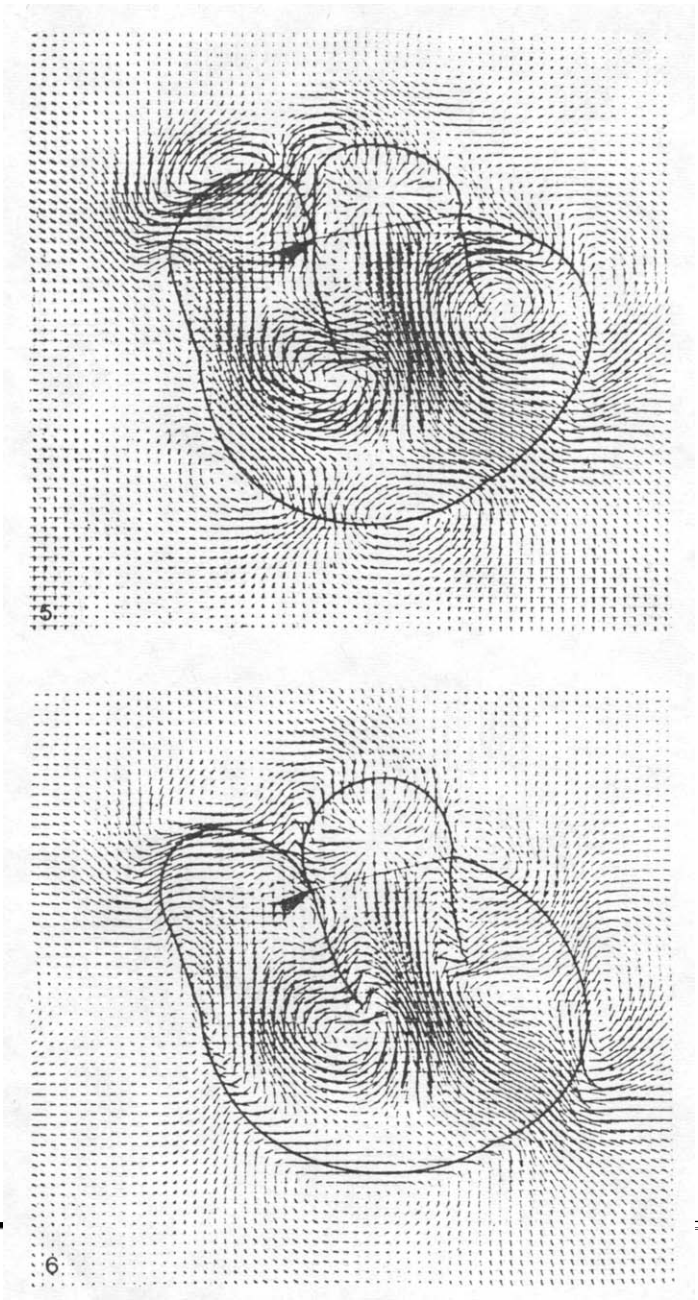

FIG. 7. *Continued.*

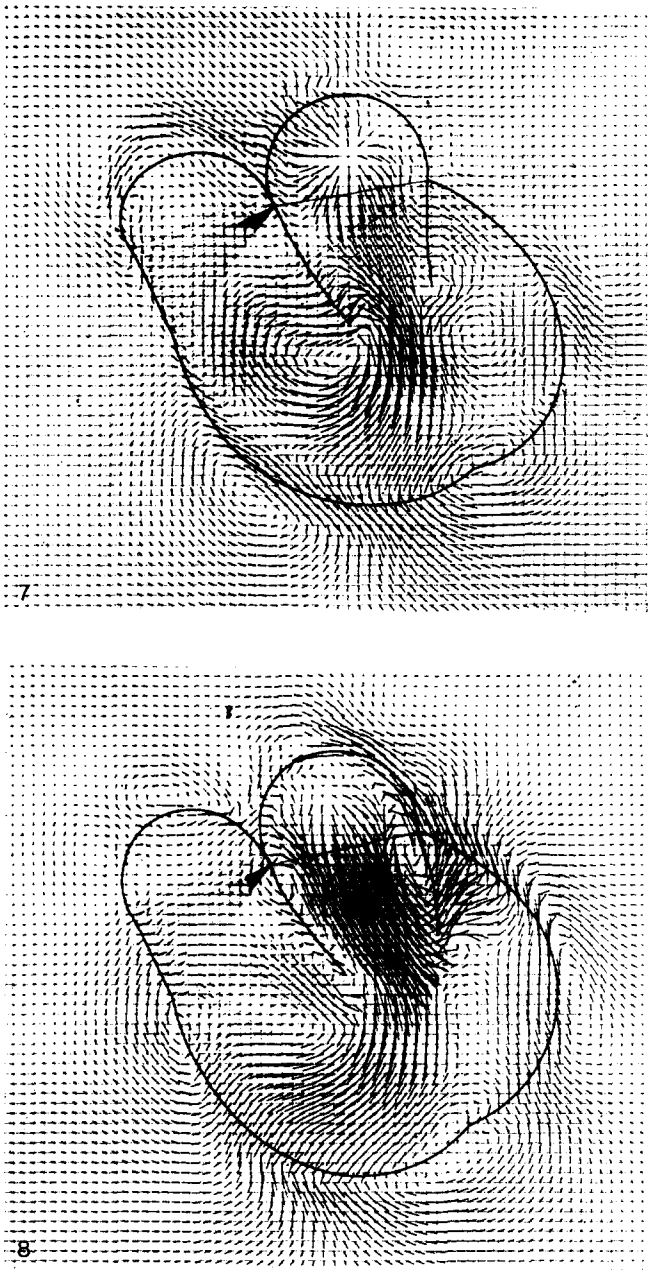

FIG. 7. *Continued.*

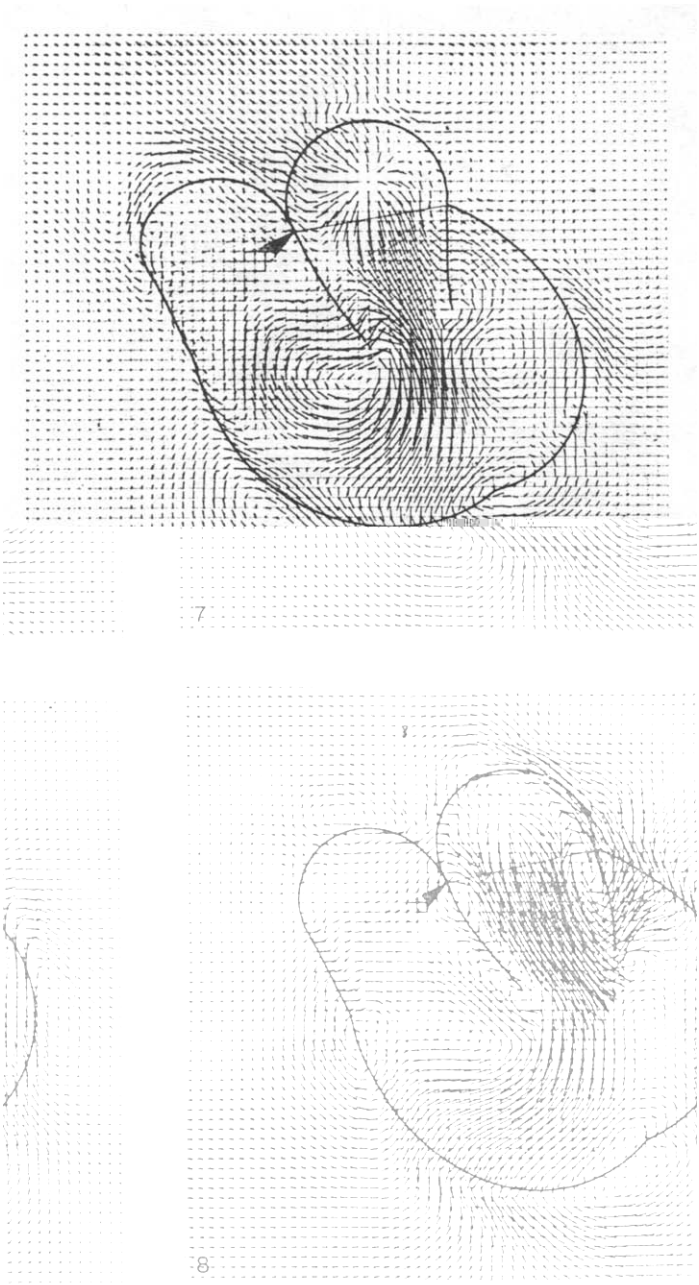

FIG. 7. *Continued.*

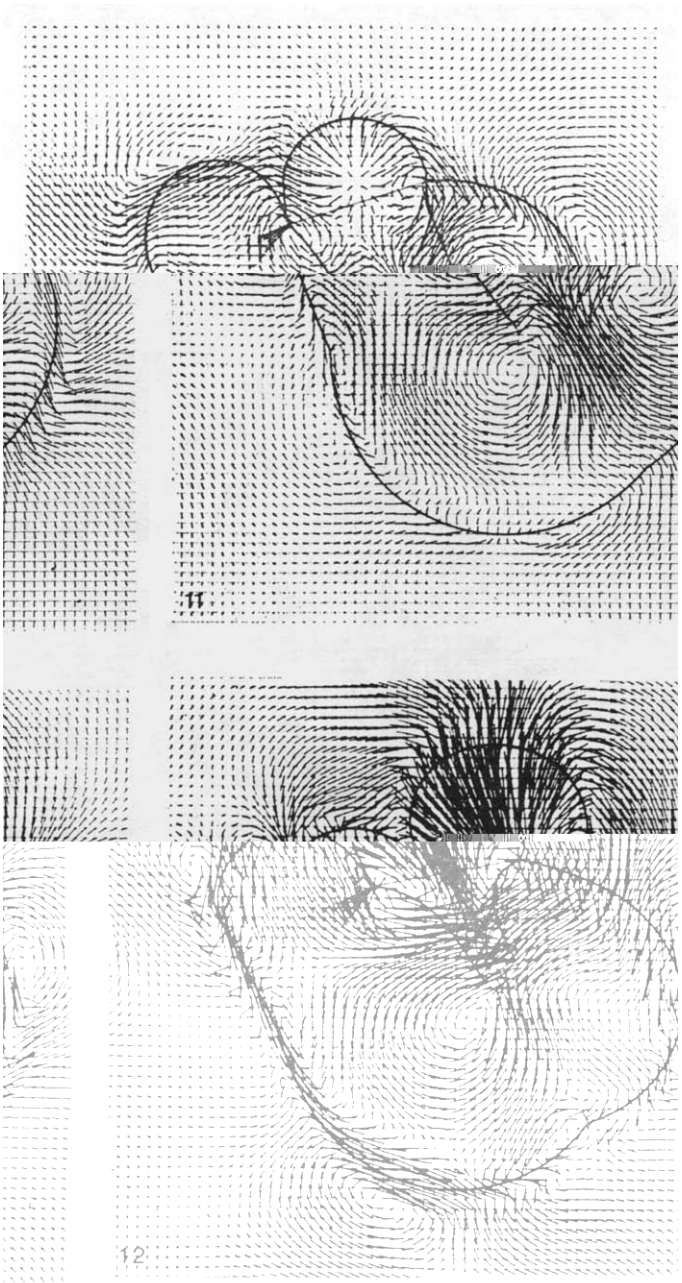

FIG. 7. *Continued.*

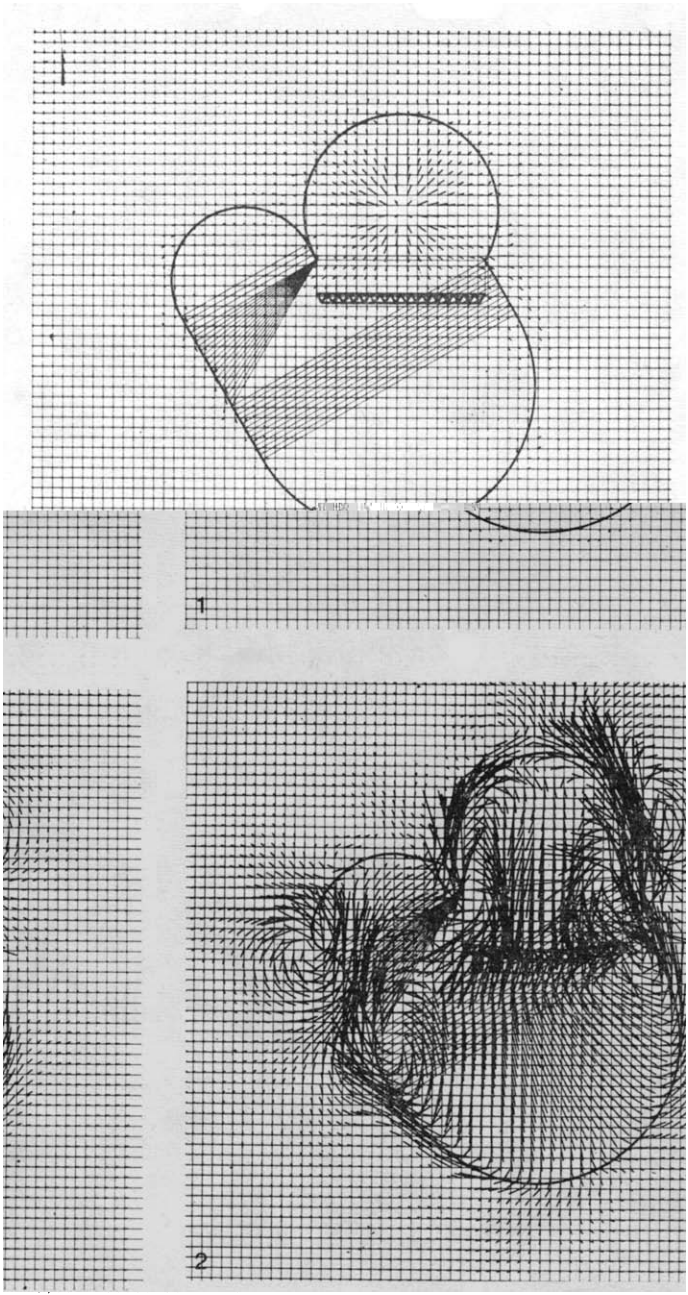

FIG. 8. Flow patterns of a prosthetic mitral valve. Timing is the same as in Fig. 7. The valve can translate open and rotate about a stop to its maximum angle of opening. Vortices form but are less effective in closing the valve. Backflow during closure is greater and involves fluid escaping past the valve as well as volume displaced.

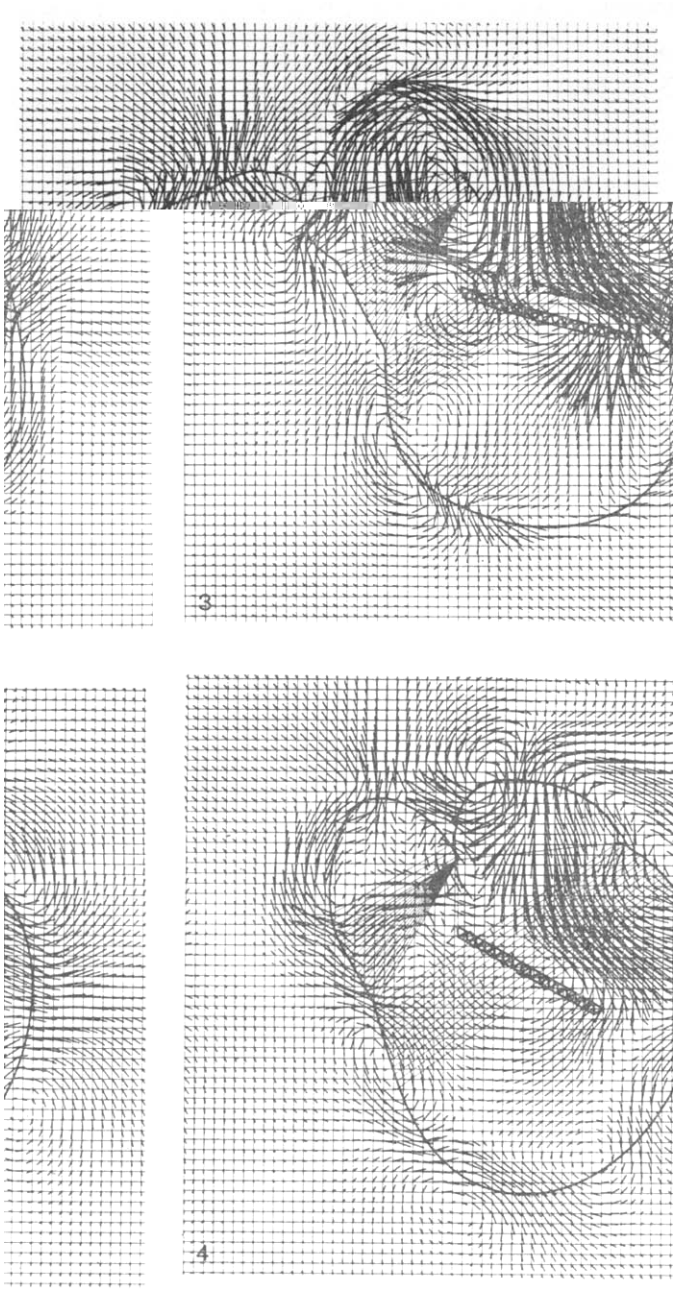

FIG. 8. *Continued.*

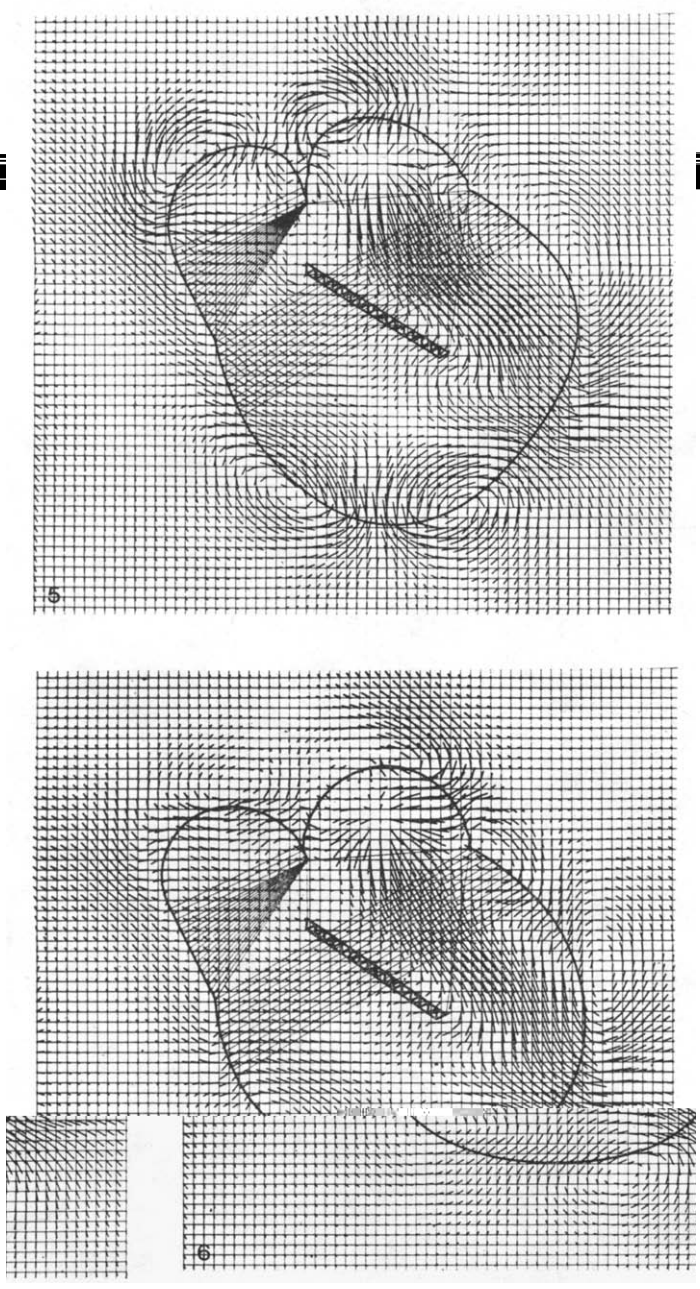

FIG. 8. *Continued.*

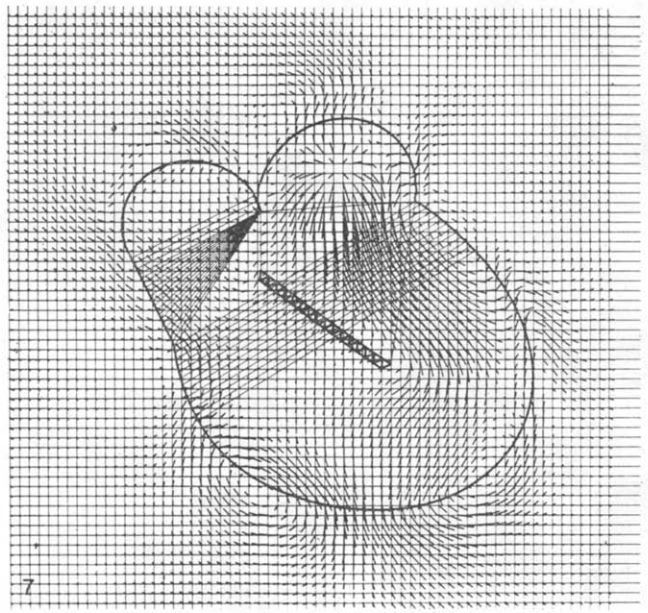

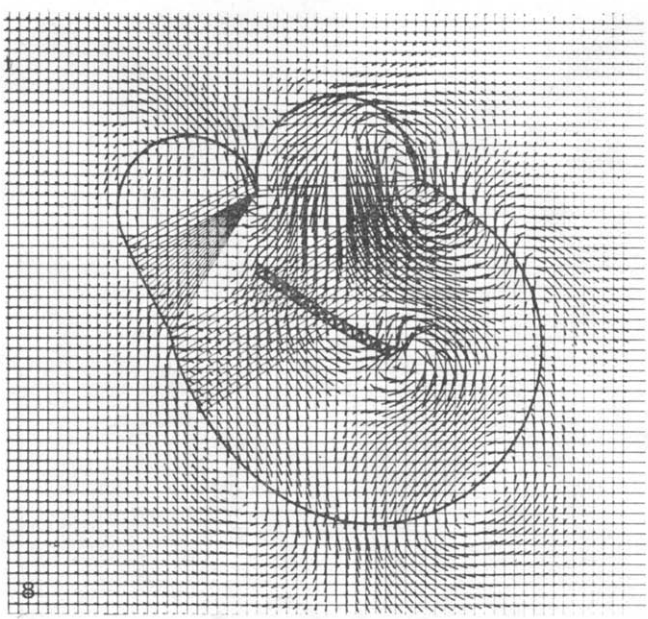

FIG. 8. *Continued.*

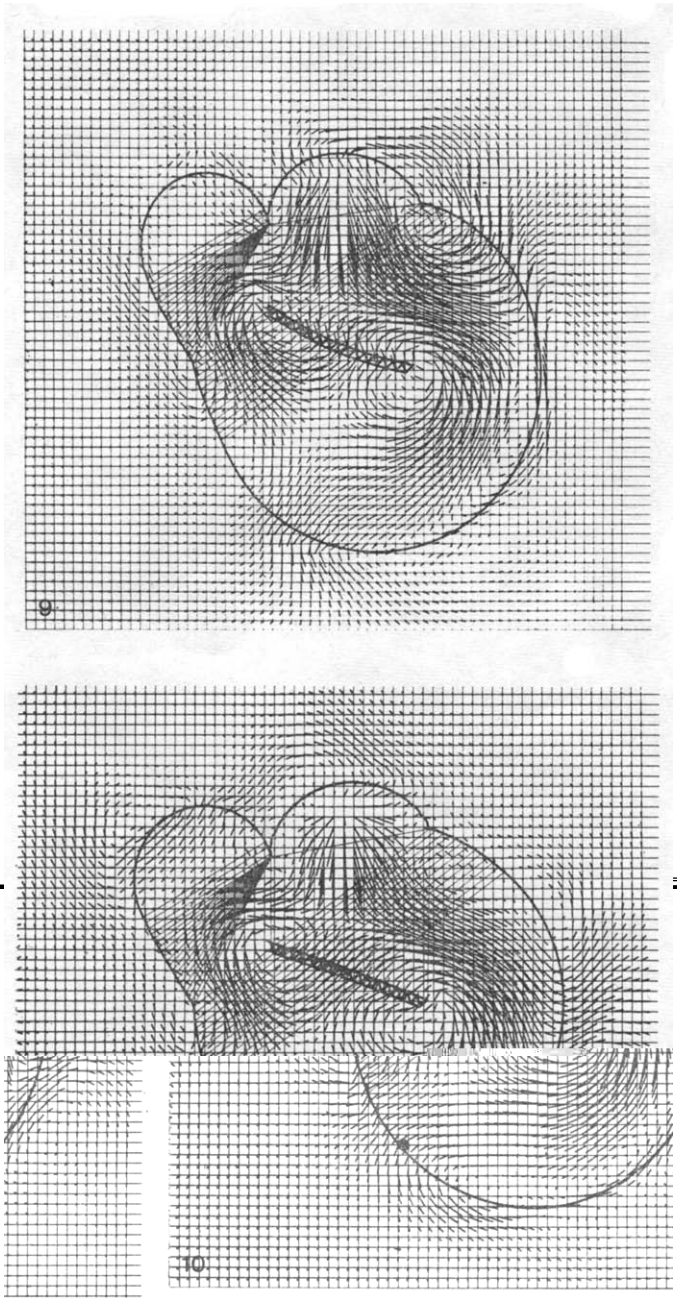

FIG. 8. *Continued.*

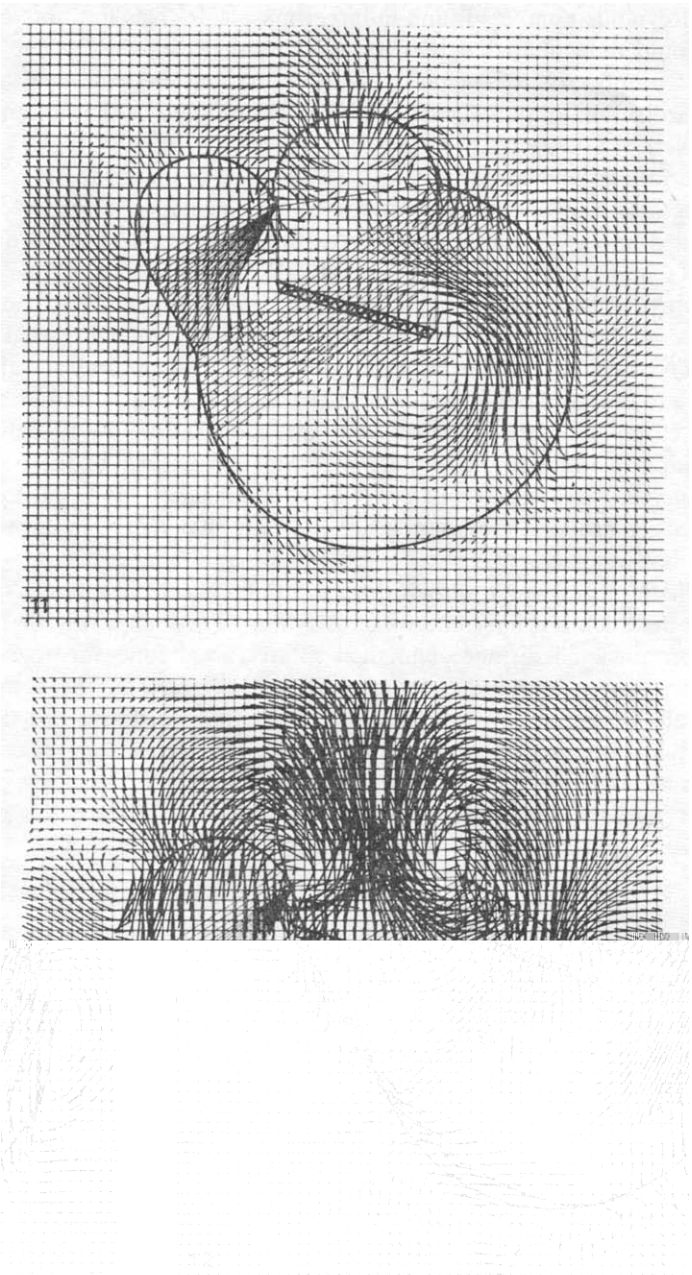

FIG. 8. *Continued.*

checked by solving the heart flow problem with a numerical scheme which is efficient even at the Reynolds numbers found in larger mammals. This has not yet been done. Also, we should remember that the lack of dependence of the cardiac flow pattern on Reynolds number (if it is a real phenomenon) may be caused by some special feature of cardiac anatomy and may therefore fail to hold in the presence of certain artificial valves.

The numerical parameters are as follows. We use a square mesh with 64 points in each direction. The part of the cardiac cycle which is of interest for the mitral valve is divided into 640 time steps. The program requires 300000_8 words of core on the CDC 6600 and takes about 2 hr. for each run.

The most useful form of output from these computational experiments is a ciné film produced by the CALCOMP 1675. In Figs. 7 and 8 we show selected frames from two such films, one for the natural and one for an artificial mitral valve. On each frame we see the instantaneous position of the heart and valve, and an array of line segments (vectors) giving the magnitude and direction of the flow at each mesh point. In interpreting these figures it is important to keep in mind that the boundaries are moving. Thus the streamlines will cross the boundaries. This does not mean that fluid particles are crossing the boundaries, but only that the boundaries are moving at the local fluid velocity.

The prosthetic mitral valve shown in Fig. 8 is an eccentric monocusp valve [14], the occluder of which is a flat plate which is mounted in such a way that it translates forward a certain fixed distance and then rotates about one end to its maximally open position. The constraints on the valve are enforced in the computation by forces generated in special links. Clearly, the translation distance and the maximum angle of opening are design parameters for this class of valves, and our computational methods can be used to study the influence of these parameters on valve performance. This has not yet been done, but it illustrates how the methods of this paper can be applied to the practical problem of valve design.

11. Conclusions

The great strength of the numerical method reported in this paper is its generality. The investigator can construct a heart and valve of arbitrary design in the computer and test their combined performance. Interventions that would be difficult to perform in the experimental animal are straightforward in the computational context. For example, one can vary the strength and timing of the atrial contraction by changing only a few cards in the computer program. If different artificial valves are to be compared, they can be tested under identical conditions without any difficulty.

The application of the method in its present form involves certain practical difficulties, however. Although the method will accommodate a heart and valve of arbitrary complexity, the work of the investigator in specifying such a structure in terms of its links is considerable. Although the method is applicable in principle to arbitrarily high Reynolds numbers and to any number of dimensions, the limitations of computer

time and available core impose severe restrictions. In particular, we are limited to two dimensions and to very low Reynolds numbers. Despite these limitations, the results bear a striking resemblance to the flow patterns and valve motions which have been reported in animal experiments [6, 11–13] and in physical models [10].

Although we have not yet attempted a quantitative comparison, we emphasize that our computational method generates certain data which may be directly compared with experiments. Among these we mention the space-averaged atrial and ventricular pressures at each instant, the instantaneous volume rate of flow through the mitral valve, and the motions of the valve leaflets. These data are available experimentally by means of pressure catheters, electromagnetic flow meters, and echocardiagrams. The value of the method, however, is that it also generates important information which would be very difficult to obtain in animal experiments. For example, the computational method gives us the flow pattern $\mathbf{u}(\mathbf{x}, t)$.

In our opinion, the difficulties mentioned above will be removed by future research. As more becomes known about the pattern of the structure of the heart wall, the task of specifying the design of a computational cardiac chamber may be considerably reduced. Also, it may become possible to remove the practical restrictions on the Reynolds number and on the number of dimensions by the use of other numerical methods for the fluid mechanical part of the calculation. The formulation of the problem and the method of representing the heart and valves in terms of a link structure may survive this transition.

ACKNOWLEDGMENTS

The author is deeply indebted to Alexandre Chorin, Edward Yellin, and Olof Widlund, who have participated in this project and whose research has made this project possible. This work was supported in part by a research grant from the National Institutes of Health, HL-17859. Computation was supported by the US ERDA under Contract EY-76-C-02-3077*000 at New York University.

REFERENCES

1. C. S. PESKIN, Flow patterns around heart valves: a numerical method, *J. Comput. Phys.* **10** (1972), 252.
2. A. J. CHORIN, Numerical solution of the Navier–Stokes equations, *Math. Comp.* **22** (1968), 745.
3. D. FISCHER, G. GOLUB, O. HALD, C. LEIVA, AND O. WIDLUND, On Fourier–Toeplitz methods for separable elliptic systems, *Math. Comp.* **28** (1974), 349.
4. C. S. PESKIN, Flow patterns around heart valves, *in* "Lecture Notes in Physics" (H. Cabannes and R. Temam, Eds.), Vol. 19, pp. 214–221, Springer-Verlag, Berlin/Heidelberg/New York, 1973.
5. C. S. PESKIN, "Flow Patterns Around Heart Valves: A Digital Computer Method for Solving the Equations of Motion," thesis, Albert Einstein College of Medicine, 1972.
6. E. L. YELLIN, R. W. M. FRATER, C. S. PESKIN, AND S. LANIADO, Left ventricular inflow patterns and mitral valve motion: Animal studies and computer analysis, *in* "Proceedings of the Fourth New England Bioengineering Conference" (S. Saha, Ed.), pp. 177–180, Pergamon Press, New York, 1976.
7. D. J. ROSE, A graph-theoretic study of the numerical solution of sparse positive definite systems

of linear equations, *in* "Graph Theory and Computing" (R. C. Read, Ed.), pp. 183–217, Academic Press, New York, 1972.

8. E. BRAUNWALD, J. ROSS, AND E. H. SONNENBLICK, "Mechanisms of Contraction of the Normal and Failing Heart," Little Brown, Boston, 1968.
9. A. F. HUXLEY, Muscle structures and theories of contraction, *Progr. Biophys.* 7 (1957), 255.
10. B. J. BELLHOUSE, Fluid mechanics of a model mitral valve and left ventricle. *Cardiovasc. Res.* **6** (1972), 199.
11. D. E. M. TAYLOR AND J. D. WADE, Pattern of blood flow within the heart: a stable system. *Cardiovasc. Res.* **7** (1973), 14.
12. S. LANIADO, E. YELLIN, M. KOTLER, L. LEVY, J. STADLER, AND R. TERDIMAN, A study of the dynamic relations between the mitral valve echogram and phasic mitral flow, *Circulation* **51** (1975), 104.
13. A. G. TSAKIRIS, D. A. GORDON, Y. MATHIEU, AND I. LIPTON, Motion of both mitral valve leaflets: a cineroentgenographic study in intact dogs, *J. Appl. Physiology* **39** (1975), 359.
14. R. W. M. FRATER, H. R. WEXLER, AND E. L. YELLIN, The in vivo comparison of hemodynamic function of ball, disk, and eccentric monocusp artificial mitral vlave, in "Prosthetic Heart Valves" (L. Brewer, Ed.), pp. 262–277, Charles C Thomas, Springfield, Ill., 1969.